Revelation and Science
Vol. 14, No. 02 (1446H/2024) 90-105

Molecular Dynamics Simulations of Glycerol-3-Phosphate Acyltransferase Protein from *Chlorella sorokiniana* with Glycerol-3-Phosphate and Oleoyl-CoA: Insights into the Synergistic Interactions

Khairul Bariyyah Abd Halim [1,2]*, Nur Hidayah Rozaidi[1],
[1] Department of Biotechnology, Kulliyah of Science, International Islamic University Malaysia, Kuantan Campus, 25200 Kuantan, Pahang, Malaysia
[2] Research Unit for Bioinformatics and Computational Biology (RUBIC), Kulliyah of Science, International Islamic University Malaysia, Kuantan Campus, 25200 Kuantan, Pahang, Malaysia.

ABSTRACT
Microalgae have the potential to accumulate high amounts of neutral lipids, specifically triacylglycerol (TAG), which can serve as a feedstock for biofuel production. In Chlorella sp., TAG synthesis is initiated by the rate-limiting enzyme Glycerol-3-Phosphate Acyltransferase (GPAT), playing a critical role in the first step of acylation using Glycerol-3-Phosphate (G3P) and acetyl-CoA. However, compared to higher plants and other eukaryotes, the lipid synthesis pathway in microalgae is not as thoroughly studied. To effectively apply genetic engineering in improving algal biofuel, a deep understanding of the molecular behaviour of GPAT and its potential binding partners is crucial for comprehending the GPAT mechanism of action. In this study, molecular dynamics simulations were conducted to investigate the complexes of GPAT, GPAT-G3P and GPAT-oleoyl-CoA. Our results revealed that G3P formed nine hydrogen bonds and six hydrophobic bonds with GPAT, while oleoyl-CoA formed seven hydrogen bonds and nine hydrophobic bonds. Analysis of the MD simulation trajectory indicated that both G3P and oleoyl-CoA were predicted to be positioned synergistically to facilitate acylation of the fatty acyl moiety to the sn1 position of G3P. Moreover, the protein-ligand complexes remained stable throughout the MD simulation, suggesting that synergistic interactions between G3P and oleoyl-CoA may occur in the bound state with GPAT, promoting the formation of lysophosphatidic acid (LPA).
Keywords: Molecular dynamics simulation, GPAT protein, *Chlorella sorokiniana*, TAG synthesis

ABSTRAK
Mikroalga mempunyai potensi untuk mengumpul jumlah lipid neutral yang tinggi, khususnya triasilgliserol (TAG), yang boleh berfungsi sebagai bahan mentah untuk pengeluaran bio-bahan api. Dalam Chlorella sp., sintesis TAG diawali oleh enzim pengehad GPAT (Glycerol-3-Phosphate Acyltransferase), yang memainkan peranan penting dalam langkah pertama pengasilan menggunakan Glycerol-3-Phosphate (G3P) dan asetil-CoA. Walau bagaimanapun, berbanding dengan tumbuhan tinggi dan eukariota lain, laluan sintesis lipid dalam mikroalga tidak dikaji sepenuhnya. Untuk mengaplikasikan kejuruteraan genetik secara berkesan dalam meningkatkan bio-bahan api berasaskan alga, pemahaman yang mendalam tentang tingkah laku molekul GPAT dan molekul yang bergabung dengannya adalah penting untuk memahami mekanisme tindakan GPAT. Dalam kajian ini, simulasi dinamik molekul telah dijalankan untuk menyiasat kompleks GPAT, GPAT-G3P dan GPAT-oleoil-CoA. Keputusan kami mendedahkan bahawa G3P membentuk sembilan ikatan hidrogen dan enam ikatan hidrofobik dengan GPAT, sementara oleoil-CoA membentuk tujuh ikatan hidrogen dan sembilan ikatan hidrofobik. Analisis lintasan simulasi MD menunjukkan bahawa kedua-dua G3P dan oleoil-CoA diramalkan berada secara sinergistik untuk memudahkan asilasi moieti asil lemak ke posisi sn1 G3P. Selain itu, kompleks protein-ligand tetap stabil sepanjang simulasi MD, menunjukkan bahawa interaksi sinergistik antara G3P dan oleoil-CoA mungkin berlaku dalam keadaan terikat dengan GPAT, menggalakkan pembentukan asid lisofosfatidik (LPA).
Kata Kunci: Simulasi dinamik molekul, protein GPAT, Chlorella sorokiniana, sintesis TAG

**Corresponding author:*
Khairul Bariyyah Abd Halim
Kiulliyyah of Science,
International Islamic University Malaysia
Email: ***kbariyyah@iium.edu.my***

1.0 INTRODUCTION

According to the World Population Prospects 2019 by the United Nations (UN), Department of Economic and Social Affairs (DESA), the global population is projected to increase from 7.7 billion people in 2019 to 10.9 billion in 2100. This significant growth is accompanied by various challenges, including energy crisis, increased emissions of toxic gases, drastic climate changes, global warming, and greenhouse effects (Alishah Aratboni et al., 2019). Consequently, addressing these concerns and developing renewable energy sources to meet the rising global energy demand while mitigating environmental impacts is crucial (Arora et al., 2018). Therefore, the development of alternative fuels derived from renewable sources has become essential. These fuels include biomethane from algal biomass through anaerobic digestion (Bohutskyi et al., 2019), biodiesel from algal oil, bioethanol from carbohydrates (Tiwari & Kiran, 2018), and marine microalgae sugars, such as seaweed (Moshood et al., 2021).

Microalgae, which are single-celled photosynthetic organisms, have the capability to convert carbon dioxide and light into biomass and possess a high lipid content (Alishah Aratboni et al., 2019). Their rapid growth rates allow them to thrive without arable land and with reduced amounts of freshwater, making them an attractive option for biofuel production (Alishah Aratboni et al., 2019; Arora et al., 2018; Mulgund, 2022). Heterotrophic cultivation of microalgae can result in the accumulation of high levels of fatty acids (FAs), which are essential for lipid production for biodiesel (Patel et al., 2022). Under stress conditions such as excessive carbon sources and nutrient deficiencies, microorganisms convert carbon into fatty acids and store them as triacylglycerols (TAGs) for energy (Younes et al., 2020). Previous research has shown that TAGs are the primary form of energy storage in microalgae, constituting 60–70% of their dry cell weight (Hu et al., 2008; Scott et al., 2010).TAG biosynthesis in microalgae occurs within the endoplasmic reticulum (ER) through two pathways: the acyl-CoA dependent pathway and the acyl-CoA-independent pathway. The primary pathway for TAG biosynthesis in microalgae is the acyl-CoA dependent pathway, known as the Kennedy pathway. This pathway begins with the acylation of glycerol-3-phosphate (G3P) by acyl-CoA:glycerol-3-phosphate acyltransferase (GPAT)to produce lysophosphatidic acid (LPA). The LPA is further acylated by acyl-CoA-dependent acyl-CoA: LPA acyltransferase (LPAAT) to form phosphatidic acid (PA). Phosphatidic acid phosphatase (PAP) dephosphorylates the PA, resulting in the formation of diacylglycerol (DAG). Finally, diacylglycerol (DAG) is converted to TAG through a catalytic process by acyl-CoA:DAG acyltransferase (DGAT). In the acyl-CoA-independent pathway, phospholipid:DAG acyltransferases (PDATs) utilize phosphatidylcholine (PC) as an acyl donor to produce TAG from DAG. Once TAG synthesis is complete, it is sequestered into lipid droplets (LDs), which consist of a phospholipid monolayer and a hydrophobic core that stores neutral lipids, primarily TAGs (Chen and Wang, 2021) see Figure 1.

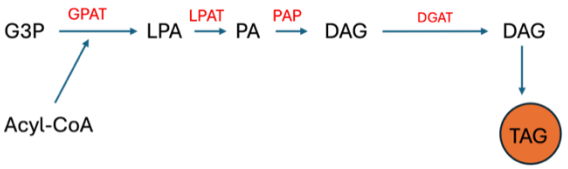

Figure 1 Glycerol phosphate pathway for de novo triacylglycerol (TAG) and glycerophospholipid synthesis. GPAT, glycerol-3-phosphate acyltransferase; LPA, lysophosphatidic acid; PA, phosphatidic acid; DAG, diacylglycerol; DGAT, diacylglycerol acyltransferase

.

The GPAT enzyme holds a crucial role in the synthesis of TAGs and determines the lipid content in microalgal cells (Chen and Wang, 2021). A study found that when the GPAT gene from *Lobosphaera incisa* was expressed in *Chlamydomonas reinhardtii*, TAG biosynthesis increased by 50% (Iskandarov et al., 2016). The GPAT protein is involved in the initial step of TAG biosynthesis, catalyzing the formation of PA from acyl-CoA. Consequently, suppressing GPAT expression may lead to a reduction in lipid content in microalgal cells (Wang et al., 2018). Given its role in initiating TAG biosynthesis, the GPAT protein shows promise as a target for gene manipulation in microalgae to enhance oil production (Misra and Panda, 2013). Additional studies have explored the impact of altering gene expression levels in the lipid biosynthesis pathway on lipid accumulation in microalgal cells (Rawat et al., 2022). Furthermore, research has demonstrated that reduced expression of GPAT9 in Arabidopsis thaliana affects the composition and quantity of TAGs in seeds (Shockey et al., 2016). Hence, the GPAT protein is crucial for optimizing lipid productivity in microalgal cells. While extensive research has been conducted on the GPAT enzyme in mammalian and plant species, limited attention has been given to the GPAT structure in microalgal species, specifically *Chlorella sp*. (Misra and Panda, 2013). Multiple genome-wide analyses have been performed on the GPAT enzyme in seven microalgae, including diatoms (*Phaeodactylum tricornutum and Thalassiosira pseudonana*), green algae (*Chlamydomonas reinhardtii, Volvox carteri, Ostreococcus lucimarinus, and Ostreococcus tauri),* and red algae (*Cyanidioschyzon merolae*) (Misra and Panda, 2013; Waschburger et al., 2018). Nevertheless, the GPAT protein from *Chlorella sp*. has not been structurally characterized thus far. Consequently, computational studies are indispensable for comprehending lipid biosynthesis and augmenting oil yield from *Chlorella sp.*

In this study we focused on *Chlorella sorokiniana*, a microalgal species commonly found in Malaysia freshwater. *C. sorokiniana* possesses favorable fatty acid profiles for biodiesel production, including palmitic acid (C16:0), stearic acid (C18:0), oleic acid (C18:1), linoleic acid (C18:2), and α-linolenic acid (C18:3n3) (Cha et al., 2011). Following the findings of Cha et al. (2011), oleic acid was selected as the suitable fatty acid for this study. Our research aim was to explore the potential mechanism underlying the acylation of glycerol-3-phosphate (G3P) and the production of lysophosphatidic acid (LPA) by acyl-CoA: glycerol-3-phosphate acyltransferase (GPAT) in *Chlorella sorokiniana* , utilizing a molecular dynamics simulation approach. We conducted molecular dynamics simulations of the previously docked complex involving GPAT with G3P and GPAT with oleyl-CoA (an acyl-CoA with the acyl group derived from oleic acid).

2. MATERIAL AND METHOD

2.1 Structure Preparation

The 3D structures of the GPAT-G3P and GPAT-oleoyl-CoA complexes were obtained from a previous study (Mohd Fuzi, 2021). In the study, the 3D structure of the GPAT protein were obtained using homology modelling technique using *Cucurbita moshata* structure (PDB ID :1K30 and 1IUQ, with 1.9 Å and 1.5 Å resolution respectively).

2.2 Molecular dynamics (MD) simulations

2.2.1 GPAT-G3P system

The molecular dynamics (MD) simulations were conducted to evaluate the stability and conformation of the docked protein-ligand complexes. The MD simulations were conducted on three separate systems: (1) GPAT and G3P complex, and (2) GPAT and oleoyl-CoA complex. MD simulation and energy minimization were performed using GROMACS 2018.8 (Abraham et al., 2015) by adopting the GROMOS 53a7 force field and analyze using built-in GROMACS utilities. Meanwhile, Automated Topology Build (ATB) Repository, a web-accessible server used to generate ligand topology file (https://atb.uq.edu.au/) (Malde et al., 2011). The protein-ligand complex was maintained under a boundary environment using a 10 Å distance from the box edges to the protein, and a single point charge (SPC) solvent model was utilized to solvate the system individually. Next, the overall charge of the system was neutralized by individually adding counter ions to the system (Mandal et al.,2019).

Subsequently, an energy minimization phase with the steepest descent algorithm of 50,000 steps was conducted to relax the system. For the equilibration phase, the ligand and protein were restrained, and the temperature was set constant at 300 K along with a pressure of 1 atm for 25,000 steps over 50 picoseconds (ps) of time-step integration. After the equilibration steps were completed for each system at the desired pressure and temperature, MD production was performed for 100 nanoseconds (ns) at 310 K and 1 atm pressure. The MD run parameters had two femtoseconds (fs) of time-step integration. The simulation was conducted in triplicate. For analysis, the trajectories were saved every 100 ps (Mandal et al., 2019). These procedures were conducted using both the GPAT in apo form and GPAT-G3P systems.

2.2.2 GPAT-oleyl-CoA

For GPAT-oleoyl-CoA, the CHARMM-GUI online server (https://www.charmm-gui.org/) was utilized to set up the MD simulation parameter file. In CHARMM-GUI, a solution builder generator is used to generate the input files for the MD simulation of our desired molecule in an aqueous environment. This generator solvates, adds ions, and neutralizes the system, thus producing the input files for MD simulations (Jo et al., 2008; Lee et al., 2016; Lee et al., 2020). Then, the MD simulation on GROMACS was performed after CHARMM-GUI generated the input files. An energy minimization phase of 5,000 steps was conducted using the steepest descent algorithm. Next, the equilibration phase of 125,000 steps was conducted with 1 fs time step integration. MD was run for 100 ns with constant temperature and pressure values of 303.15 K and 1 atm, respectively. Furthermore, the MD trajectories were saved every 100 ps for analysis. Different program was used to setup the MD simulation system for GPAT-G3P and GPAT-oleoyl-CoA complexes due to the difficulty in getting the correct parameter for the ligand. The simulation were performed at constant temperature for both system.

2.3 Trajectory Analysis

For the analysis, the protein-ligand complex stability was evaluated by the changes in the radius of gyration, pair distance, hydrogen bond (hbond), and by computing the root-mean-square deviation (RMSD) and root-

mean-square fluctuation (RMSF) for the atom groups in the protein complex. The structures and trajectories obtained during the simulation were visualized using the PyMol (Schrödinger and DeLano, 2020) tool package (Justino et al., 2021). The binding interactions within protein complexes were viewed and obtained using the BIOVIA Discovery Studio Visualizer (Discovery Studio Visualizer v21.1.0.20298) and LigPlot+ v.2.2.7 (Laskowski and Swindells, 2011).

3. RESULT AND DISCUSSION

Protein-ligand complex stability

Molecular dynamics simulation is a valuable tool for understanding the binding manner and interatomic interactions between the GPAT protein and both G3P and oleoyl-CoA. The Root Mean Square Deviation (RMSD) was computed to monitor the stability of the system during the simulation. A smaller deviation indicates a higher potential for the protein conformational structure to become more stable during the simulation process (Singh, 2020). Overall, all three replicates of the protein complexes reached a plateau phase with small deviations at some point in the MD simulation, indicating that the protein conformational structures were stabilized throughout the MD simulations. The RMSD graphs in Figure 2(b) showed that the GPAT-G3P complex reached stability early in the MD simulation. All three replicates of the GPAT-G3P complex exhibited smaller fluctuations from the initial state and reached stability with an average RMSD value of 0.3567 nm (3.567 Å) and standard deviation (SD) of 0.0297 nm (0.2 Å) . Meanwhile, for the GPAT-oleoyl-CoA complex, two of the replicates reached equilibrium at around 15 ns, while one replicate reached equilibrium at around 30 ns with an average RMSD of 0.5787 nm (5.787 Å) and SD = 0.0900847 nm (0.9 Å) for the triplicates (Figure 2 (c)).

The ligand's root mean square deviation (RMSD) was calculated to assess changes in its binding pose during the simulation. This assessment helps determine the quality of the ligand topology and indicates the stability of protein-ligand interactions. Additionally, poor ligand topology can disrupt native interactions, leading to distortions in binding positions (Lemkul, 2019). As shown in Figure 3, the RMSD graphs for both G3P and oleoyl-CoA ligands show how their conformational structures reached stability early on in the MD simulation. The G3P structure has smaller fluctuations from their initial stage and reached stability at RMSD values below 2 Å in all triplicates. On the other hand, the oleoyl-CoA ligand conformational structures reached stability at RMSD of ~1 Å after 40 ns

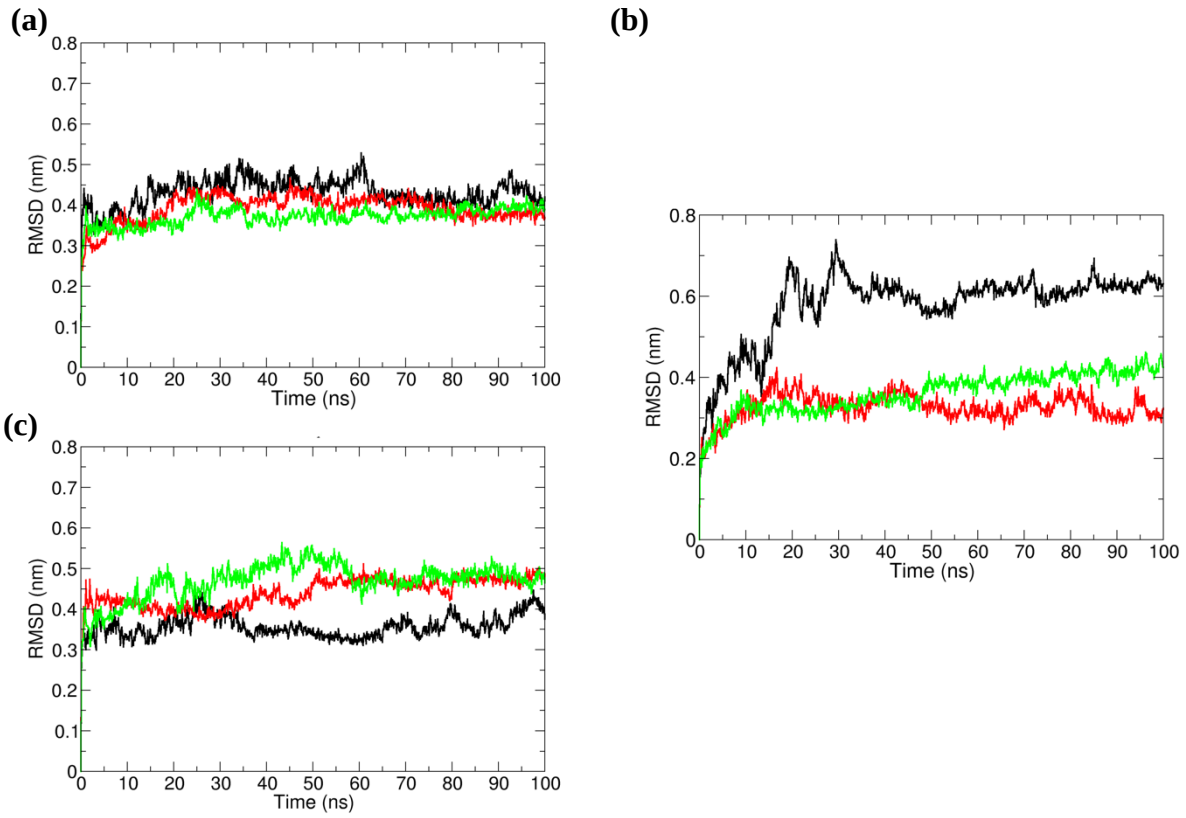

Figure 2 RMSD graph of systems for (a) GPAT protein(apo-form), (b) GPAT-G3P complex, and (c) GPAT-Oleoyl-CoA complex in triplicate manner. Black – first run, Red – second run and Green – third run. 1 nm = 10 Å

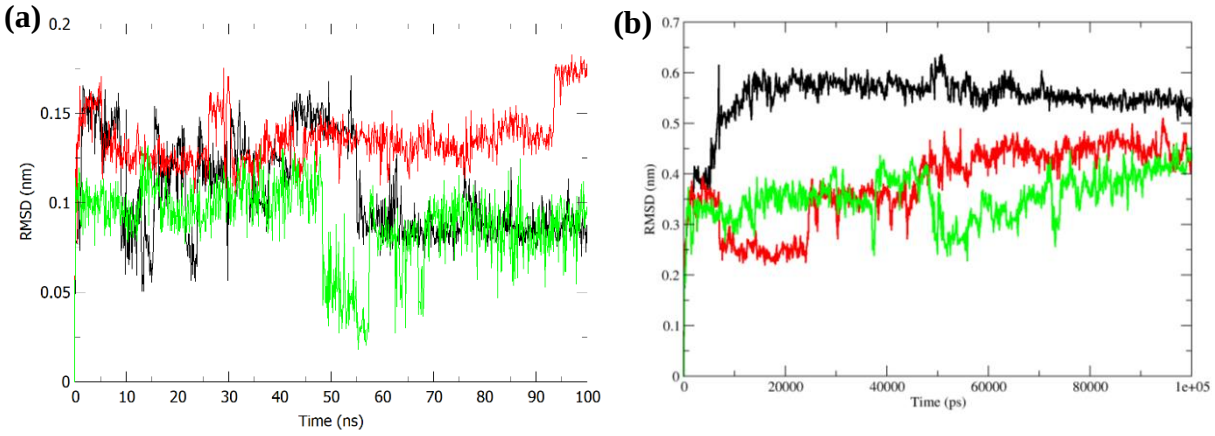

Figure 3 The RMSD graphs of ligands for (a) G3P and (b) oleoyl-CoA in triplicates.

Molecular Binding Interactions of GPAT Protein Complex with G3P and Oleoyl-CoA

Hydrogen bonds play a crucial role in the non-covalent interactions that contribute to the formation of protein-ligand complexes. The analysis of hydrogen bonding revealed that, on average, G3P formed 2 to 10 hydrogen bonds, while oleoyl-CoA formed 1 to 8 hydrogen bonds during the 100 ns simulation. The pair distance profiles were generated using the GROMACS pairdist

module, which calculated the minimum or maximum distances between a reference selection and one or more other selections. In this study, we determined the distances between the active site of the GPAT protein and the ligands (G3P and oleoyl-CoA). The results showed that G3P remained closer to the active site, with a value of approximately 1.5 Å, compared to Oleoyl-CoA, which was approximately 1.8 Å. Furthermore, neither ligand moved more than 2.3 Å away from the active site throughout the simulation.

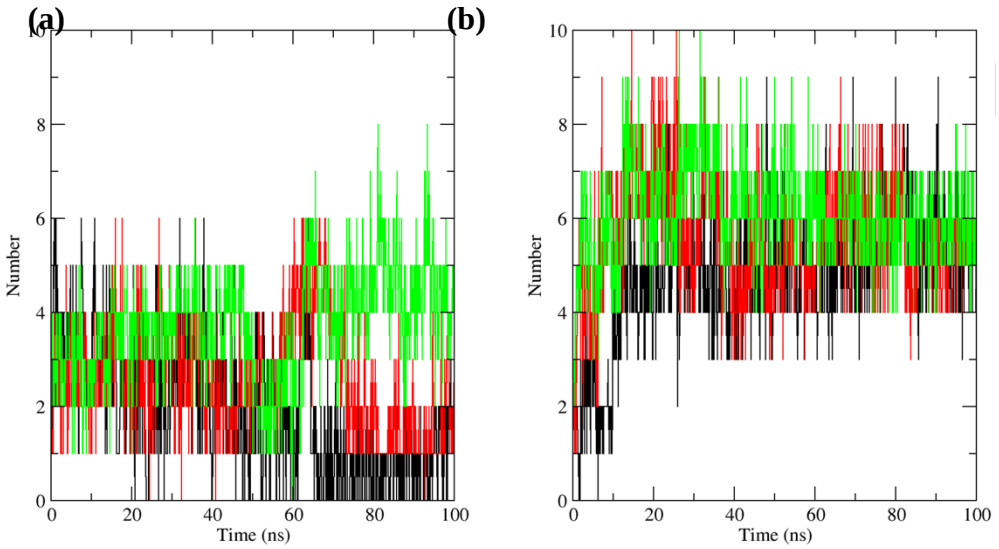

Figure 4 H-bond profile for (a) GPAT-G3P complex and (b) GPAT-Oleoyl-CoA complex in triplicate manner. Black – first run, Red – second run and Green – third run.

The number of hydrogen bonds formed by the complexes can serve as an indication of the driving forces behind the binding process (Bitencourt-Ferreira and de Azevedo, 2019). G3P exhibited hydrogen bond interactions with GPAT residues Glu144, Glu144, His141, His141, Ala145, Asp146, Asp146, Val168, and Gly170, as summarized in Table 1. In addition, oleoyl-CoA demonstrated hydrogen bond interactions with Asp171, Asp171, Arg172, Arg172, Ser193, Gly235, and Gly235. The hydrogen bond involving Val168 is at a distance of 3.31 Å, which could suggest that the bond is relatively weak since its distance exceeds 3.0 Å. Only two residues, His141 and Asp146, were found in the conserved region of GPAT that were involved in hydrogen bond interactions with both ligands. The characteristics of the hydrogen bonds formed between GPAT, G3P, and oleoyl-CoA are summarized and presented in Table 1. Furthermore, visual representations of the interactions between G3P and oleoyl-CoA with GPAT are depicted in Figure 5.

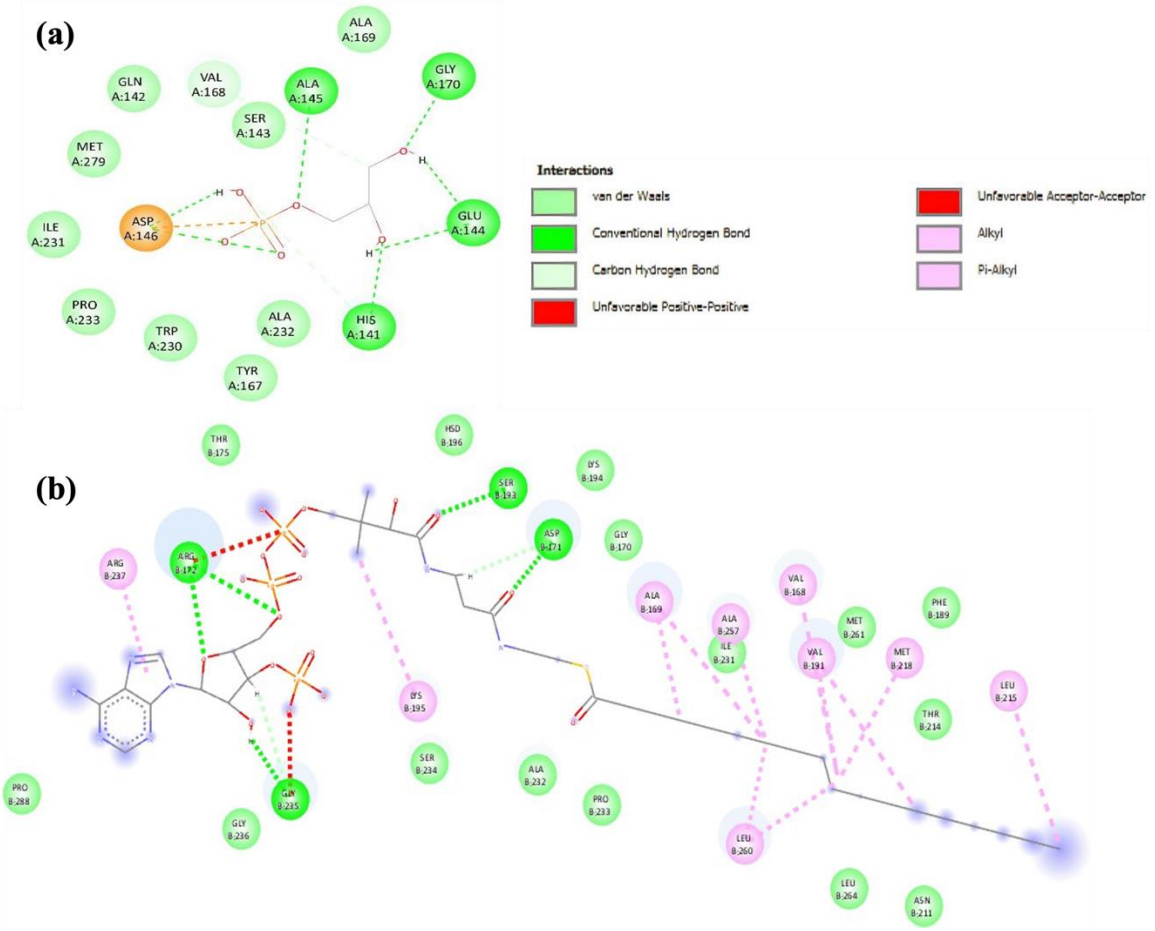

Figure 5 (a) Two-dimensional (2D) schematic diagram of the hydrogen bond interactions of the GPAT-G3P complex obtained from BIOVIA Discovery Studio. (b) The 2D schematic diagram of hydrogen bond interactions of the GPAT-oleoyl-CoA complex obtained from BIOVIA Discovery Studio.

Hydrogen bonds are the second most common bond interactions within protein-ligand complexes, which strengthen the establishment of the protein-ligand binding interactions (Ferreira De Freitas and Schapira, 2017). Moreover, hydrogen bonds play a major role in providing mechanical and structural stability to protein systems and protein-ligand complexes. The role of hydrogen bonds includes the exchange of protein-water interactions for protein-protein and water-water interactions (Ferenczy and Kellermayer, 2022). Additionally, the heavy atoms found in hydrogen bonds are separated by a similar median distance of 3.0 Å thus making the bond stronger when it is less than 3.0 Å (Ferreira De Freitas and Schapira, 2017).

Table 1 Number of hydrogen bonds, binding energies, and amino acid consensus of GPAT with G3P and oleoyl-CoA.

Ligands	GPAT Protein		
	Number of Hydrogen Bond	H-bond Distance	Interacting Residues
G3P	9	1.45 Å	Glu144
		1.70 Å	Glu144
		1.76 Å	His141
		3.75 Å	His141
		2.48 Å	Ala145
		1.63 Å	Asp146
		2.01 Å	Asp146
		3.31 Å	Val168
		1.65 Å	Gly170
Oleoyl- CoA	7	2.89 Å	Asp171
		2.66 Å	Asp171
		2.11 Å	Arg172
		2.63 Å	Arg172 Ser193
		1.80 Å	
		1.73 Å	Gly235
		2.94 Å	Gly235

LigPlot+ was utilized to determine the hydrophobic interactions among GPAT, G3P, and oleoyl-CoA. The hydrophobic interactions within the protein complexes are visualized in 2D schematic diagrams in Figure 6 and presented in tabular form in Table 2. G3P exhibited six interacting residues (Ala145, Tyr167, Val168, Ala169, Trp230, and Pro233), while oleoyl-CoA displayed nine interacting residues (Ala169, Asp171, Lys195, Hsd196, Thr214, Leu215, Ala232, Arg237, and Leu260). Of these hydrophobic interactions observed in both ligands, only three are involved in the conserved region of GPAT: Lys195, Hsd196, and Arg237.

Hydrophobic interactions are the predominant interactions in the protein-ligand complex (Ferreira De Freitas and Schapira, 2017). Optimized hydrophobic interactions contribute to the stabilization of ligands at their target sites, thereby enhancing binding affinity and drug efficacy. These interactions, such as π-stacking, alkyl, and π-π alkyl interactions, play a vital role in protein folding by maintaining stability, exhibiting biological activity, and minimizing interactions with water (Patil et al., 2010). Additionally, the hydrophobic surface of proteins is typically situated within the hydrophobic core, serving as a major driving force for protein folding due to the substantial gain in free energy resulting from these interactions (Ferenczy and Kellermayer, 2022). Furthermore, hydrophobic interactions are recognized as the main factor in increasing ligand efficiency (Ferreira De Freitas and Schapira, 2017). This suggests that oleoyl-CoA may be a more efficient ligand compared to G3P, as it possesses nine hydrophobic interacting residues, whereas G3P has only six.

Synergistic interactions between glycerol-3-phosphate (G3P) and oleoyl-CoA in glycerol-3-phosphate acyltransferase (GPAT).

The representative structure obtained from molecular dynamics trajectories using cluster analysis was utilized to compare the binding mode and binding orientation of the ligand in both GPAT-G3P and GPAT-oleoyl-CoA complexes (Figure 7). It was observed that G3P and oleoyl-CoA stably bound in close proximity to each other, while positioning themselves in their most favourable positions for mutual interaction, as depicted in Figure 8

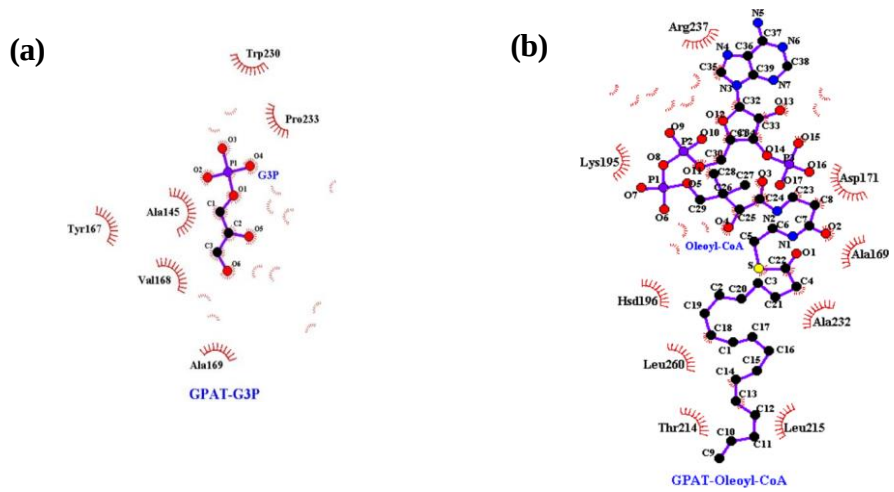

Figure 6 Ligplot+ analysis results. 2D schematic of the hydrophobic interactions of GPAT with ligands (a) G3P and (b) oleoyl-CoA. The interacting residues are shown in red spiked arcs, making hydrophobic contact with the ligands, which are shown in purple

Table 2 Hydrophobic Interacting residues of G3P and oleoyl-CoA with GPAT.

Ligands	Number of Residues	Interacting Residues
G3P	6	Ala145, Tyr167, Val168, Ala169, Trp230, and Pro233
Oleoyl-CoA	9	Ala169, Asp171, Lys195, Hsd196, Thr214, Leu215, Ala232, Arg237, and Leu260

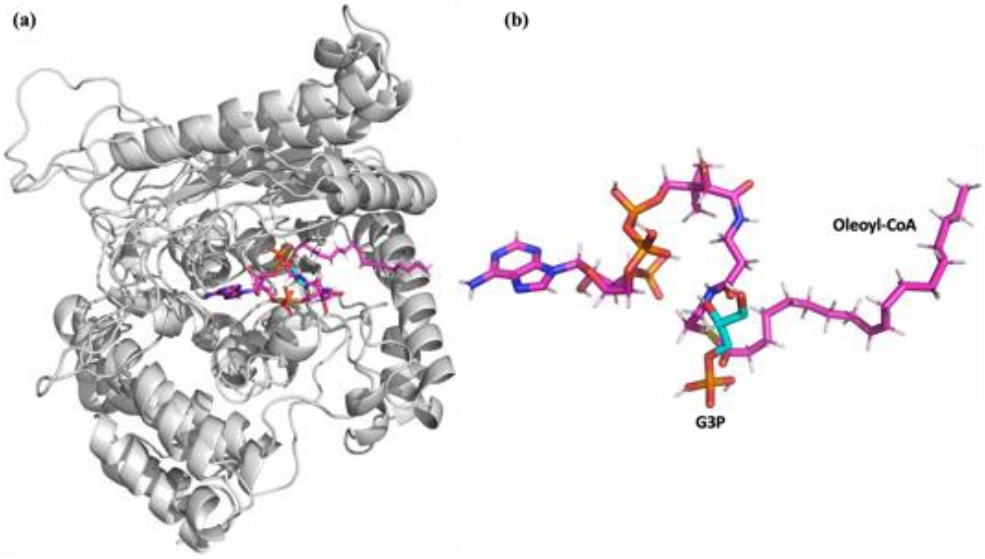

Figure 8 (a) Cluster analysis of the aligned GPAT-G3P and GPAT-oleoyl-CoA complexes at 0.1 nm cut-off. (b) Extracted G3P and oleoyl-CoA from aligned protein complexes. Cyan – G3P and Pink – Oleoyl-CoA.

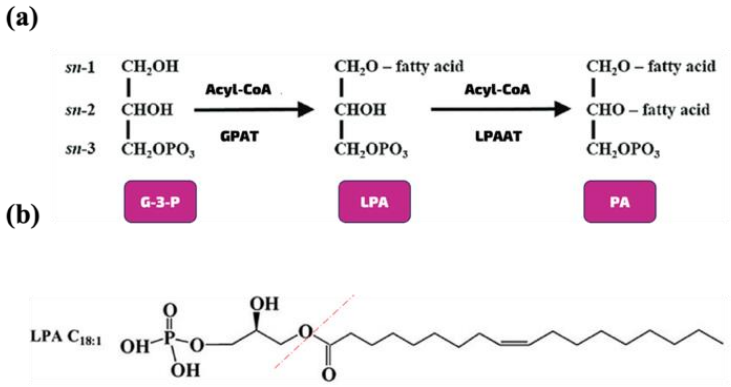

Figure 9 (a) A general mechanism of LPA formation by Acyl-CoA:GPAT and PA formation by LPAAT. (b) 2D schematic diagram of LPA formation via acylation of the fatty acid moiety in oleoyl-CoA to the sn-1 position in G3P by oleoyl-CoA:GPAT (Cho et al. 2019) as indicated by the red dotted line.

A closer inspection of the protein-ligand complex revelaed that the C^1-hydroxyl group of G3P (sn-1) interacts with the O^2 of coenzyme A from oleoyl-CoA, which is located near the oleate side of acyl-CoA. The synthesis of lysophosphatidic acid (LPA) and phosphatidic acid (PA) occurs when GPAT catalyzes the esterification of the fatty acid moiety from oleoyl-CoA to the sn-1 position of G3P, resulting in the formation of LPA. Subsequently, further acylation may takes place through the action of oleoyl-CoA:LPA acyltransferase (LPAAT), which transfers the acyl moiety to the sn-2 position of G3P and generates PA (Cho et al., 2019). Figure 9 presents a 2D schematic illustrating the initial acylation of G3P to form LPA.

CONCLUSION

Our study suggests that G3P and oleoyl-CoA did not complete for the same binding site on GPAT as they form VDW and hydrogen bond interactions with different residues. In addition, the most frequently occurring structures obtained from the clustering analysis of the MD trajectories for both GPAT-G3P and GPAT-oleoyl-CoA revealed that G3P and oleoyl-CoA were positioned in proximity for mutual interaction. Overall, our results suggest that G3P and oleoyl-CoA may interact synergistically to promote the acylation of G3P, leading to the formation of LPA.

Acknowledgement

This study is sponsored by FRGS15-207-0448.

REFERENCES

Abraham, M. J., Murtola, T., Schulz, R., Páll, S., Smith, J. C., Hess, B., & Lindah, E. (2015). Gromacs: High performance molecular simulations through multi-level parallelism from laptops to supercomputers. *SoftwareX*, *1–2*, 19–25. https://doi.org/10.1016/j.softx.2015.06.001

Alishah Aratboni, H., Rafiei, N., Garcia-Granados, R., Alemzadeh, A., & Morones-Ramírez,
J. R. (2019). Biomass and lipid induction strategies in microalgae for biofuel production and other applications. *Microbial Cell Factories*, *18*(1), 1–17. https://doi.org/10.1186/s12934-019-1228-4

Arora, N.; Pienkos, P. T., Pruthi, V., Poluri, K. M., & Guarnieri, M. T. (2018). Leveraging algal omics to reveal potential targets for augmenting TAG accumulation. *Biotechnology Advances*, *36*(4), 1274–1292. https://doi.org/10.1016/j.biotechadv.2018.04.005

Bitencourt-Ferreira, G., & de Azevedo, W. F. (2019). Docking with SwissDock. In *Methods in Molecular Biology* (Vol. 2053). https://doi.org/10.1007/978-1-4939-9752-7_12

Bohutskyi, P., Keller, T. A., Phan, D., Parris, M. L., Li, M., Richardson, L., & Kopachevsky,
A. M. (2019). Co-digestion of wastewater-grown filamentous algae with sewage sludge improves biomethane production and energy balance compared to thermal, chemical, or thermochemical pretreatments. *Frontiers in Energy Research*, *7*(JUN), 1–19. https://doi.org/10.3389/fenrg.2019.00047

Cha,T.S., Chen,J.W., Goh,E.G., Aziz,A., & Loh, S.H. (2011). Differential regulation of fatty acid biosynthesis in two Chlorella species in response to nitrate treatments and the potential of binary blending microalgae oils for biodiesel application. *Bioresource Technology*, *102(220)*, 10633-10640.

Chen, H., & Wang, Q. (2021). Regulatory mechanisms of lipid biosynthesis in microalgae.
Biological Reviews, *96*(5), 2373–2391. https://doi.org/10.1111/brv.12759

Cho, H. J., Choi, S. H., Kim, H. J., Lee, B. H., Rhim, H., Kim, H. C., … Nah, S. Y. (2019). Bioactive lipids in gintonin-enriched fraction from ginseng. *Journal of Ginseng Research*, *43*(2), 209–217. https://doi.org/10.1016/j.jgr.2017.11.006

Elgharbawy, A. S., Sadik, W. A., Sadek, O. M., & Kasaby, M. A. (2021). A review on biodiesel feedstocks and production technologies. *Journal of the Chilean Chemical Society*, *66*(1), 5098–5109. https://doi.org/10.4067/S0717-97072021000105098

Ferreira De Freitas, R., & Schapira, M. (2017). A systematic analysis of atomic protein- ligand interactions in the PDB. *MedChemComm*, *8*(10), 1970–1981. https://doi.org/10.1039/c7md00381a

Ferenczy, G. G., & Kellermayer, M. (2022). Contribution of hydrophobic interactions to protein mechanical stability. *Computational and Structural Biotechnology Journal*, *20*, 1946–1956. https://doi.org/10.1016/j.csbj.2022.04.025

Hu, Q., Sommerfeld, M., Jarvis, E., Ghirardi, M., Posewitz, M., Seibert, M., & Darzins, A. (2008). Microalgal triacylglycerols as feedstocks for biofuel production: Perspectives and advances. *Plant Journal*, *54*(4), 621–639. https://doi.org/10.1111/j.1365-313X.2008.03492.x

Iskandarov, U., Sitnik, S., Shtaida, N., Didi-Cohen, S., Leu, S., Khozin-Goldberg, I., Boussiba, S. (2016). Cloning and characterization of a GPAT-like gene from the microalga Lobosphaera incisa (Trebouxiophyceae): overexpression in Chlamydomonas reinhardtii enhances TAG production. *Journal of Applied Phycology*, *28*(2), 907–919.

Jo, S., Kim, T., Iyer, V. G., & Im, W. (2008). CHARMM-GUI: A Web-Based Graphical User Interface for CHARMM. *Journal of Computational Chemistry*, *29*, 1859–1865. https://doi.org/10.1002/jcc.20945

Justino, G. C., Nascimento, C. P., & Justino, M. C. (2021). Molecular dynamics simulations and analysis for bioinformatics undergraduate students. *Biochemistry and Molecular Biology Education*, *49*(4), 570–582. https://doi.org/10.1002/bmb.21512

Laskowski, R. A., & Swindells, M. B. (2011). LigPlot+: Multiple Ligand-Protein Interaction Diagrams for Drug Discovery. *Journal of Chemical Information and Modeling*, *51*, 2778–2786.
Singh, D. B. (2020). *Computer-Aided Drug Design*. Springer.

Lee, J., Cheng, X., Swails, J. M., Yeom, M. S., Eastman, P. K., Lemkul, J. A., … Im, W. (2016). CHARMM-GUI Input Generator for NAMD, GROMACS, AMBER, OpenMM, and CHARMM/OpenMM Simulations Using the CHARMM36 Additive Force Field. *Journal of Chemical Theory and Computation*, *12*(1), 405–413. https://doi.org/10.1021/acs.jctc.5b00935

Lee, J., Hitzenberger, M., Rieger, M., Kern, N. R., Zacharias, M., & Im, W. (2020). CHARMM-GUI supports the Amber force fields. *Journal of Chemical Physics*, *153*(3). https://doi.org/10.1063/5.0012280

Lemkul, J. (2019). From Proteins to Perturbed Hamiltonians: A Suite of Tutorials for the GROMACS-2018 Molecular Simulation Package [Article v1.0]. *Living Journal of Computational Molecular Science*, *1*(1), 1–53. https://doi.org/10.33011/livecoms.1.1.5068

Malde, A. K., Zuo, L., Breeze, M., Stroet, M., Poger, D., Nair, P. C., … Mark, A. E. (2011). An Automated Force Field Topology Builder (ATB) and Repository: Version 1.0. *Journal of Chemical Theory and Computation*, *7*(12), 4026–4037.

Mandal, H., Vijayakumar, S., Yadav, S., Kumar Singh, S., & Das, P. (2019). Validation of NAD synthase inhibitors for inhibiting the cell viability of Leishmania donovani: In silico and in vitro approach. *Journal of Biomolecular Structure and Dynamics*, *37*(17), 4481–4493. https://doi.org/10.1080/07391102.2018.1552199

Misra N, Panda PK. (2013). In search of actionable targets for agrigenomics and microalgal biofuel production: sequence-structural diversity studies on algal and higher plants with a focus on GPAT protein. OMICS. Apr;17(4):173-86. doi: 10.1089/omi.2012.0094.

Mosood, T.D., Nawanir,G., & Mahmud, F.(2021). Microalgae biofuels production: A microalgal biofuel production: A systematic review on socioeconomic prospects of microalgae biofuels and policy implications. *Environmental Challenges*, 5 (May),1002017.

Mulgund, A. (2022). Increasing lipid accumulation in microalgae through environmental manipulation, metabolic and genetic engineering: a review in the energy NEXUS framework. *Energy Nexus*, *5*(June 2021), 100054. https://doi.org/10.1016/j.nexus.2022.100054

Nur Fatini, M. F. (2021). *In silico Molecular Modeling and Simulation Studies of Glycerol-3-Phosphate acyltransferase (GPAT) protein from Chlorella sp. on Understanding of lipid synthesis.* (BSc dissertation). International Islamic University Malaysia.

Patel, A., Krikigianni, E., Rova, U., Christakopoulos, P., & Matsakas, L. (2022). Bioprocessing of volatile fatty acids by oleaginous freshwater microalgae and their potential for biofuel and protein production. *Chemical Engineering Journal*, *438*(March), 135529. https://doi.org/10.1016/j.cej.2022.135529

Rawat, J., Gupta, P. K., Pandit, S., Priya, K., Agarwal, D., Pant, M., … Pande, V. (2022). Latest Expansions in Lipid Enhancement of Microalgae for Biodiesel Production: An Update. *Energies*, *15*(4), 1550. https://doi.org/10.3390/en15041550

Schrödinger, L., & DeLano, W. (2020). PyMOL. Retrieved from http://www.pymol.org/pymol

Shockey, J., Regmi, A., Cotton, K., Adhikari, N., Browse, J., & Bates, P. D. (2016). Identification of arabidopsis GPAT9 (At5g60620) as an essential gene involved in triacylglycerol biosynthesis1[OPEN]. *Plant Physiology*, *170*(1), 163–179. https://doi.org/10.1104/pp.15.01563

Scott, S. A., Davey, M. P., Dennis, J. S., Horst, I., Howe, C. J., Lea-Smith, D. J., & Smith, A. G. (2010). Biodiesel from algae: Challenges and prospects. *Current Opinion in Biotechnology*, *21*(3), 277–286. https://doi.org/10.1016/j.copbio.2010.03.005

Tiwari, A., & Kiran, T. (2018). Biofuels from Microalgae. *Intech*, 13. Retrieved from http://dx.doi.org/10.1039/C7RA00172J%0Ahttps://www.intechopen.com/books/advance d-biometric-technologies/liveness-detection-in-biometrics%0Ahttp://dx.doi.org/10.1016/j.colsurfa.2011.12.014

Wang, H., Zhang, Y., Zhou, W., Noppol, L., & Liu, T. (2018). Mechanism and enhancement of lipid accumulation in filamentous oleaginous microalgae Tribonema minus under heterotrophic condition 06 Biological Sciences 0601 Biochemistry and Cell Biology. *Biotechnology for Biofuels*, *11*(1), 1–14. https://doi.org/10.1186/s13068-018-1329-z

Waschburger, E., Kulcheski, F. R., Veto, N. M., Margis, R., Margis-Pinheiro, M., & Turchetto-Zolet, A. C. (2018). Genome-wide analysis of the glycerol-3-phosphate acyltransferase (GPAT) gene family reveals the evolution and diversification of plant GPATs. *Genetics and Molecular Biology, 41*(1), 355–370. https://doi.org/10.1590/1678- 4685-gmb-2017-0076

Younes, S., Bracharz, F., Awad, D., Qoura, F., Mehlmer, N., & Brueck, T. (2020). Microbial lipid production by oleaginous yeasts grown on Scenedesmus obtusiusculus microalgae biomass hydrolysate. *Bioprocess and Biosystems*

Article History
Received: 7 February 2024
Accepted: 1 December 2024